Paper No. T6-2.9, pp. 1-5

15th INTERNATIONAL SYMPOSIUM on POWER ELECTRONICS - Ee 2009
XV Međunarodni simpozijum Energetska elektronika – Ee 2009
NOVI SAD, REPUBLIC OF SERBIA, October 28th - 30th, 2009

BEHAVIOR OF INDUCTION MOTOR DRIVES DUE TO UNSYMMETRICAL VOLTAGE SAGS

Milutin Petronijević, Nebojša Mitrović, Vojkan Kostić, Bojan Banković
University of Niš, Faculty of Electronic Engineering, Niš, Republic of Serbia

Abstract: *This paper analyses the influence of unsymmetrical voltage sags on the increase of torque and speed deviation induction motor adjustable speed drives (ASDs). The three following general types of ASD control are analysed: scalar-controlled (V/Hz), rotor-field-oriented (RFO) and direct-torque-controlled (DTC). The analytical expressions for variations of dc link voltage and torque ripple are derived first, and incorporated into the corresponding drive models. Afterwards, the presented theoretical results for the deterioration of ASD performance due to voltage sags are validated experimentally.*

Key Words: ***Power Quality, Voltage Sag, Induction Motor Drives, Speed and Torque Deviation***

1. INTRODUCTION

Voltage sags (dips) are power quality problems with the most often appearances in public power supply network. Sensitivity of ASDs to voltage sags was a subject of numerous studies and experimental researches (e.g. [1]). In continuous process applications, stop electric drives may occur due to deviations in the speed and/or electromagnetic torque. Majority of the previous works was, concentrated only on determining sensitivity limits related to disconnection/tripping of analysed or tested ASDs due to the activation of their overcurrent/undervoltage protection systems.

The paper researches behaviour of scalar controlled (V/Hz), rotor field oriented (RFO) and direct torque controlled (DTC) induction motor (IM) drives in speed and torque controlled application in voltage sags circumstances. Analytical results, presented in this paper, show differences in behaviour of electrical drives, depending on the applied control algorithm, and suggest opportunities for improvement in practical applications. Some experimental results are shown to illustrate the obtained theoretical results.

2. VOLTAGE SAGS EFFECTS

Unbalanced voltage sags are of particular importance during the assessment of equipment sensitivity, as they are usually caused by single-line-to-ground faults (SLGFs), which are the most frequent types of system fault (responsible for around 70% of all faults, [2]). As one or two-phase voltages of SLGF-caused unbalanced single-phase and two-phase voltage sags are either unaffected, or with only a minor reduction in magnitude. During sag, ASD dc link voltage may, depending on the magnitude and duration of the experienced unbalanced sags, remain above the undervoltage protection limit. Numerous measurements around the world ([3]) point to the fact that the expected value of the remaining voltage during the sags is closer to the upper limit (between 50% and 90% of nominal voltage). Frequency converter of the some manufacturer will not lead to failure, but it will certainly lead to performance deterioration. Figure 1 illustrates the distribution of the voltage sags and also refers to the fact that they usually last for a few seconds.

Based on [2] it is known that SLGF's can produce B type sags with the depth in range of h=0 ... 1, while C and D types voltage sags depths are in range h=0.333...1. Phase voltage equations in complex form and the appropriate phasor diagrams that illustrate the above basic unsymmetrical sag types were given in Table 1. In this paper, the analysis was conducted precisely for these types of voltage sags, although similar conclusions can be drawn for the case of other types, but in case of voltage unbalance.

In case of B, C or D voltage sag input rectifiers pass into single phase operations with the consequences as input current distortion and DC voltage ripple decrease with dominant component at 100Hz and with average voltage reduction in C type voltage sag case. DC bus voltage $v_{dc}(t)$ in case of a voltage sag supply conditions, having in mind [4] is presented as:

$$v_{dc}(t) = V_{DC} + V_{DC2}\cos(2\omega_1 t + \theta_2) \qquad (1)$$

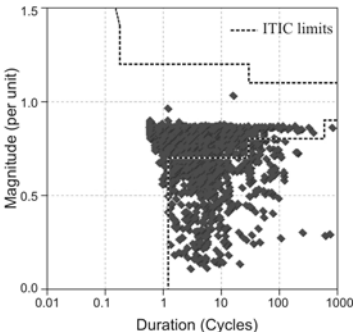

Fig. 1. *Magnitude/duration chart of voltage sags (adopted from www.i-grid.com [3])*

Table 1. *Basic types of unsymmetrical voltage sags*

Sag type	Phasor diagram solid lines during fault	Phase-to-neutral voltages (*h* designates remain voltage in p.u.)
B	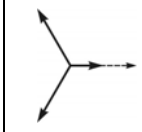	$U_a = hU$ $U_b = -(1/2)U - j(\sqrt{3}/2)U$ $U_c = -(1/2)U + j(\sqrt{3}/2)U$
C	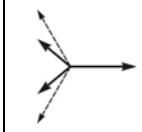	$U_a = U$ $U_b = -(1/2)U - j(\sqrt{3}/2)hU$ $U_c = -(1/2)U + j(\sqrt{3}/2)hU$
D	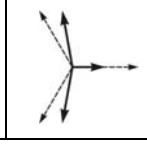	$U_a = hU$ $U_b = -(1/2)hU - j(\sqrt{3}/2)U$ $U_c = -(1/2)hU + j(\sqrt{3}/2)U$

where V_{DC} presents an average voltage value, V_{DC2} is the second voltage harmonic, ω_i is power supply angular frequency ($2\pi 50\text{s}^{-1}$ or $2\pi 60\text{s}^{-1}$) and θ_2 is an appropriate angle of the second harmonic component referring to *d*-axis which defines point on wave at sag initiation.

In general case, modulation signals can be represented:

$$u_i(t) = u_i^*(t) + e(t) \tag{2}$$

where $e(t)$ is injected harmonic (also represents direct transformation SVPWM into carrier based PWM), and $u_i^*(t)$ are called fundamental signals for appropriate phase voltages (i=a, b, c). Fundamental components of line to neutral output PWM voltages are:

$$\begin{aligned} u_{an}(t) &= \frac{1}{2}v_{dc}(t)\cdot[m\cdot\cos(\omega_s t+\varphi)+e_i(t)] \\ u_{bn}(t) &= \frac{1}{2}v_{dc}(t)\cdot[m\cdot\cos(\omega_s t-\frac{2\pi}{3}+\varphi)+e_i(t)] \\ u_{cn}(t) &= \frac{1}{2}v_{dc}(t)\cdot[m\cdot\cos(\omega_s t+\frac{2\pi}{3}+\varphi)+e_i(t)] \end{aligned} \tag{3}$$

where ω_s - inverter output fundamental frequency with modulation index m. Phase angle φ corresponds to initial phase voltage angle related to d axis.

Combining equations (2) and (3), and applying coordinate transformations, induction motor stator voltages in *dq* reference frame that rotates at a synchronous reference speed ω_s, are:

$$\begin{aligned} u_{ds}(t) &= \frac{1}{2}m\left[V_{DC}\cos\varphi + V_{DC2}\cos(2\omega_i t+\theta_2)\cos\varphi\right] \\ u_{qs}(t) &= \frac{1}{2}m\left[V_{DC}\sin\varphi + V_{DC2}\cos(2\omega_i t+\theta_2)\sin\varphi\right] \end{aligned} \tag{4}$$

In equations above the second term is a direct consequence of dc link voltage ripple because of rectifier single-phase operation.

3. THEORETICAL ANALYSIS AND ASD BEHAVIOR COMPARISONS

Assuming magnetic linearity, the equivalent two-phase model of the symmetrical IM, represented in the synchronous rotating reference frame, is:

$$u_{ds} = R_s i_{ds} - \omega_s\psi_{qs} + \frac{d}{dt}\psi_{ds} \tag{5}$$

$$u_{qs} = R_s i_{qs} + \omega_s\psi_{ds} + \frac{d}{dt}\psi_{qs} \tag{6}$$

$$0 = R_r i_{dr} - (\omega_s-\omega_m)\psi_{qr} + \frac{d}{dt}\psi_{dr} \tag{7}$$

$$0 = R_r i_{qr} + (\omega_s-\omega_m)\psi_{dr} + \frac{d}{dt}\psi_{qr} \tag{8}$$

The relations between *dq* flux linkage and currents are:

$$\begin{aligned} &\psi_{ds} = L_s i_{ds} + M i_{dr},\ \psi_{qs} = L_s i_{qs} + M i_{qr} \\ &\psi_{dr} = L_r i_{dr} + M i_{ds},\ \psi_{qr} = L_r i_{qr} + M i_{qs} \end{aligned} \tag{9}$$

Electromagnetic torque can be calculated using the following formula:

$$T_e = 1.5P(M/L_r)(i_{qs}\psi_{dr} - i_{ds}\psi_{qr}), \tag{10}$$

Voltages given by equation (4) correspond to three-phase voltages with terms ω_s, $2\omega_i+\omega_s$ and $-2\omega_i+\omega_s$. In steady state condition, solving equations (5) - (8) in case of voltage given by equations (4), and applying the superposition theorem, we obtain expressions for the *dq* stator currents:

$$i_{ds} = i_{ds0} + I_{ds2}\cos(2\omega_i t+\delta_{ds}) \tag{11}$$

$$i_{qs} = i_{qs0} + I_{qs2}\cos\left(2\omega_i t+\delta_{qs}\right), \tag{12}$$

where average stator current components are given by:

$$i_{ds0} = K_0\left[g_0\cos\varphi - b_0\sin\varphi\right], \text{ and}$$
$$i_{qs0} = K_0\left[g_0\sin\varphi + b_0\cos\varphi\right].$$

Magnitudes of additional oscillatory stator current components are (for simplicity it will be θ_2=0):

$$I_{ds2} = K_1\sqrt{|y_1|^2+|y_2|^2+2|y_1||y_2|\cos(2\varphi+\angle y_1+\angle y_2)} \tag{13}$$

$$I_{qs2} = K_1\sqrt{|y_1|^2+|y_2|^2+2|y_1||y_2|\cos(2\varphi+\angle y_1+\pi-\angle y_2)}\ . \tag{14}$$

The values of certain coefficients in the previous equations are:

$$K_0 = \frac{1}{2}mV_{DC},\ K_1 = \frac{1}{4}mV_{DC2}$$

$$y_0 = g_0 + jb_0 = \left[r_s + j\omega_s L_{ls} + \left\{j\omega_s M \| (r_r/s_0 + j\omega_s L_{lr})\right\}\right]^{-1}$$

$$y_1 = \left[r_s + j\omega_1 L_{ls} + \left\{j\omega_1 M \| (r_r/s_1 + j\omega_1 L_{lr})\right\}\right]^{-1}$$

$$y_2 = \left[r_s + j\omega_2 L_{ls} + \left\{j\omega_2 M \| (r_r/s_2 + j\omega_2 L_{lr})\right\}\right]^{-1}$$

$$\omega_1 = 2\omega_i + \omega_s,\ \omega_1 = -2\omega_i + \omega_s,$$

$$s_0 = \frac{\omega_s-\omega}{\omega_1}\ s_1 = \frac{\omega_1-\omega}{\omega_1},\ s_2 = \frac{\omega_2-\omega}{\omega_2},$$

where ω denotes motor rotor angular speed, δ_{ds} and δ_{qs} represents d and q stator current components angle respect to d axis.

After combining (11) and (12), taking into account expressions (10), the torque value can be calculated in the closed form:

$$T_e = T_{e0} + T_{e2}\cos(2\omega_i t+\phi_2) + T_{e4}\cos(4\omega_i t+\phi_4), \tag{15}$$

where T_{e0} represents average torque value, T_{e2} represents the second harmonic component and T_{e4} represents the fourth harmonic components. In the following chapters will be given the discussions on the impact of individual torque and current components, depending on the type of voltage sags.

3.1. DC link voltage reduction effects

Limitations, as a consequence of the maximum output current (I_{max}) and maximum output voltage ((U_{max}) of an AC/DC converter, can be presented in the appropriate stator variable through the equations:

$$i_{qs}^2 + i_{ds}^2 \le I_{\max}^2 \text{ , and} \quad (16)$$

$$u_{qs}^2 + u_{ds}^2 \le U_{\max}^2 \quad (17)$$

Maximum output current is determined by maximum continuous current of inverter semiconductor switches or induction motor rated current, i.e. maximum allowable thermal capacity of the converter or induction motor. The maximum stator voltage depends on the available DC-link voltage v_{DC} and pulsewidth modulation (PWM) strategy ([5]).

Equation (17), in steady state and voltage limit condition, having in mind the relationships (5)-(10), can be written as:

$$A\, i_{ds}^2 + C\, i_{qs}^2 + B\, i_{ds}\, i_{qs} \le U_{\max}^2 \quad (18)$$

where:

$$A = R_s^2 + \omega_s^2 L_s^2 ,\ B = 2R_s\omega_s \frac{M^2}{L_r} \text{ and } C = R_s^2 + \omega_s^2\sigma^2 L_s^2 .$$

This voltage-limit boundary, given by (18), is an ellipse, which area and angle of major axis depend on voltage and frequency. Equation (16) in the same axis system explains a circle, so range of drive operation can be found in cross section of these two ones.

In voltage dip case, based on (18), new ellipse can be drawn responding to the reduced voltage limit, where is easily noticeable decreasing of maximum possible q-axis stator current component which corresponds to electrical torque reduction. In this case, for constant load torque, this leads to the speed regulation loss, which explicitly explains if we build adequate torque-speed characteristics.

Figure 2 shows the curves that correspond to these limits, and also drawn the trajectory of constant rotor flux and constant stator flux, which illustrates the ASDs working point with RFO and DTC control algorithm, respectively. Intersection among flux trajectories and contours that correspond to voltage and current limit restrictions give concrete electric motor drives torque/speed behaviour, depending on the applied control algorithm.

Figure 3 shows these differences for the case of voltage reduction to 80% of nominal. It should be noted the fact that adjusting the value of flux allows the correction of the maximum available torque and in some cases overcome the consequences of voltage sag. More detailed analysis is given in [5].

3.2. DC link voltage ripple effects

The presence of second harmonic in dc link voltage, as shown in equation (15), leads to appearance of additional harmonic torque, which can cause vibration and motor overheating. It should be noted the fact that the dominant, side harmonic T_{e2} depends on the output frequency and motor load which is shown in Fig. 4 (based on formula (16)).

In the case of ASDs with the RFO and DTC control, expected behaviour is significantly different. It is well known that RFO vector control has two internal, fast control loops for i_{ds} and i_{qs} currents. From the aspect of current control loops oscillatory components i_{qs2} and i_{ds2} represent external disturbances such as it is shown in Fig. 5 in continuous time domain, neglecting the sample and hold effects.

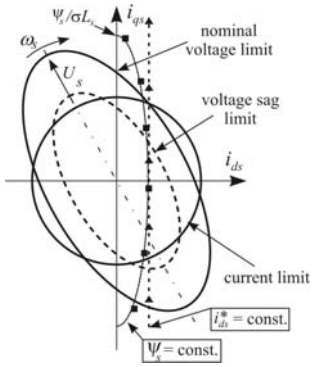

Fig. 2. *Voltage and current limits under nominal and voltage sag conditions*

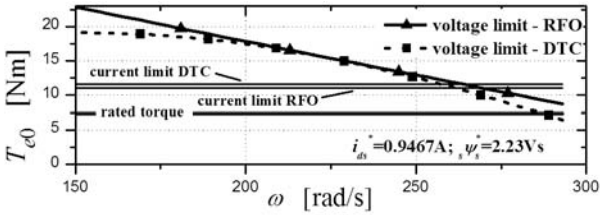

Fig. 3. *Maximum torque comparison for V_{DC}=80%V_{DCn} for RFO controlled and DTC drives*

The design of PI controller is made to cancel the machine pole $K_i/K_p=R_s/\sigma L_s$, and if a desired system bandwidth of ω_{bw} is defined, the proportional and integral gains are ([6]):

$$K_p = \sigma L_s \omega_{bw} \text{ , and} \quad (19)$$

$$K_i = R_s \omega_{bw} . \quad (20)$$

Error signal in control loop, shown in Fig. 5, can be represented as:

$$e_{iqs} = e_{ir} + e_{id} \quad (21)$$

where the e_{ir} indicates an error in tracking the reference signal i_{qs}^*; e_{id} marks the error arising from effects of the disturbance, calculated as:

$$e_{id} = -W_{i2}(s) i_{qs2} = -\frac{1}{1 + W_{PI}(s) W_q(s)} i_{qs2} \quad (22)$$

For a PI controller, whose parameters are given in (19) and (20), Bode diagram of function W_{i2} (s) is shown in Fig. 6. Increasing bandwidth of PI controller directly influence to the reduction of current amplitude oscillations while retaining basic frequency $2\omega_i$ in currents $i_{qs}(t)$ and $i_{ds}(t)$. Increasing bandwidth is necessarily accompanied by the request of increasing switching frequency, which is the limit imposed by the IGBT transistors. In the experiments, accomplished in the paper, current control loops bandwidth is set on 1250rad/s, which is mainly limited by noise presence in measured currents. For induction motor data, given in

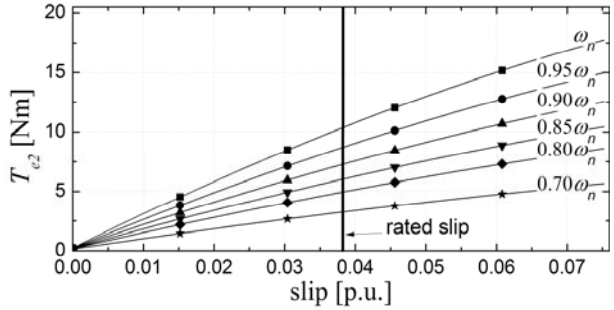

Fig. 4. *Slip and output frequency influence on torque ripple amplitude*

Table 2. *Motor data (per phase) and ASD parameters*

Rated power /speed	2200W/2835rpm
Stator voltage U_s	230V
Stator resistance R_s	2.7Ω
Stator leakage inductance L_{ls}	10.5mH
Rotor resistance R_r	2.2Ω
Rotor leakage resistance L_{lr}	10.5mH
Mutual inductance M	270mH
Motor inertia J_m	0.00184kgm^2
Total leakage coefficient σ	0.073
DC link capacitance (C_f)	2x330μF(in series)
DC link inductance (L_f)	2x3.6mH

Table 2, digital PI controller parameters for *d* and *q* current control loops are K_p=21.75 and K_i=0.768 when sample time is set to 100μs.

In the basic version, direct torque control consists of three level hysteresis comparator for torque control and two level hysteresis comparator for flux. The major problem in classical DTC control application is high value of the torque ripple, which can be overcome by switching table modification. In this paper, firstly was used modified DTC scheme with $\alpha\beta$ plane divided into twelve sectors (designated as C12DTC) instead of just six, which lead to acceptable torque ripple and stator currents distortion.

One of the favourable solutions for constant switching frequency and low torque ripple is described in [7], which is labelled as PI-DTC in this paper. Suitable torque control, in the case of constant stator flux, is achieved by setting voltage component u_{qs} in synchronous reference frame related to the stator flux. Torque control loop is shown in Fig. 7 together with the corresponding transfer functions.

In this article, PI torque controller design was done using root loci method with the help of Matlab SISO tool (Control System Toolbox) entering natural frequency ω_n and coefficient of relative damping ratio ξ. Similarly to the analysis for RFO electric drive, influence parameters of PI controller on disturbance error analysis can be explored using Bode plot diagram of function W_{T2} given by the relation:

$$e_{Td} = -W_{T2}(s)T_{e2} = -\frac{1}{1+W_{PI}(s)W_T(s)}T_{e2}. \qquad (23)$$

The coefficients of transfer function $W_T(s)$ are terms of:

$$A_1 = \frac{1.5\psi_s}{\sigma L_s};\ B_1 = \frac{R_s L_r + R_r L_s}{\sigma L_s L_r};\ B_2 = \frac{1.5\psi_s}{\sigma L_s J_m}. \qquad (24)$$

Setting parameter values natural frequency ω_n in the range from (2π100) rad/s to (2π300) rad/s, and with fixed setting ξ=0.707, Bode diagram of $W_{T2}(s)$ are drawn in Fig. 8. Having in mind the existence of induction motor parameters uncertainty and control algorithm implementation in digital form, the experiment proved that the optimal settings of parameters regulator are: K_{pT}=19.875 and K_{iT} =0.425, for torque; and $K_{p\psi}$=2500 and $K_{i\psi}$=0.425 for flux. For these controller parameters in Fig. 8 amplitude/frequency characteristic is drawn.

In the case of classical DTC with the torque (flux), hysteresis controller, whose bandwidth is infinite (practically restricted by power transistor switching speed), it is clear that the reduction of side harmonic components is almost completely, which explains the experimental results obtained later.

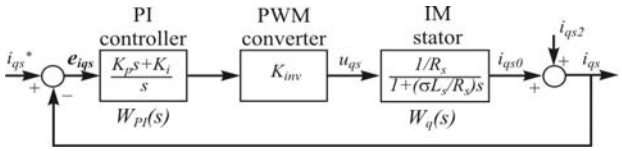

Fig. 5. *RFO controlled drives q-axis current control loop*

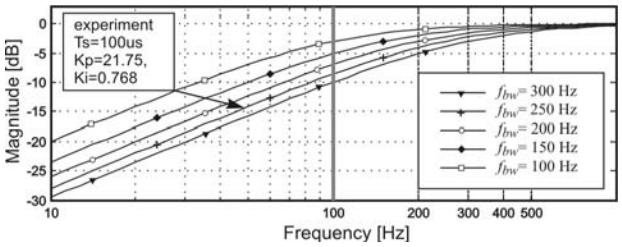

Fig. 6. *Current loop bandwidth influence on second harmonic component*

4. EXPERIMENTAL RESULTS

The first set of experiments was performed with a V/Hz ASD, controlling a motor loaded in steady state by a constant torque of 7Nm at rotational speed of 240rad/s. Shortly after the B sag (h=0) initiation, overcurrent protection was activated. In order to observe changes in relevant ASD/motor parameters without tripping the drive, motor load was, in accordance to [1], reduced to 6Nm. Figure 9 presents the effects of a single-phase type B voltage sag, obtained in experimental measurements. It can be seen that the presence of large ripples in both dc link voltage and torque (with dominant second harmonic) identified in theoretical analysis, which is also confirmed in experiments. In experiments we observed a significant distortions of the stator currents.

Afterwards, the RFO drive was tested with nearly the same rotational speed, but with the load torque equal to the rated one (7.4Nm). At time t=0.04s voltage sag was initiated. Figure 10 presents measurement results, where a significant reduction in torque ripple is evident in comparison to V/Hz controlled drive. It can be also seen that the characteristic torque harmonics occur at the same frequencies for RFO drive as for V/Hz drive, but the magnitude of the dominant 100Hz component is significantly smaller in the case of RFO drive.

DTC drives with PI controllers possess nearly the same torque closed loop bandwidth as well as RFO drives at torque producing current components control loop. Expectations regarding the torque harmonics, at the same condition as RFO drives, are reached in Fig. 11:

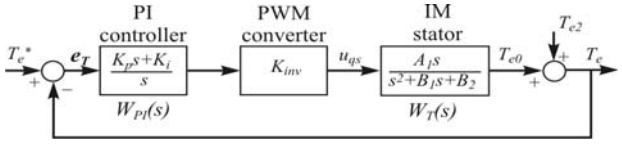

Fig. 7. *Torque control loop in PI-DTC drives*

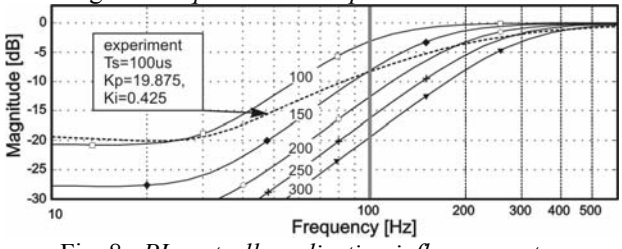

Fig. 8. *PI controller adjusting influence on torque ripple*

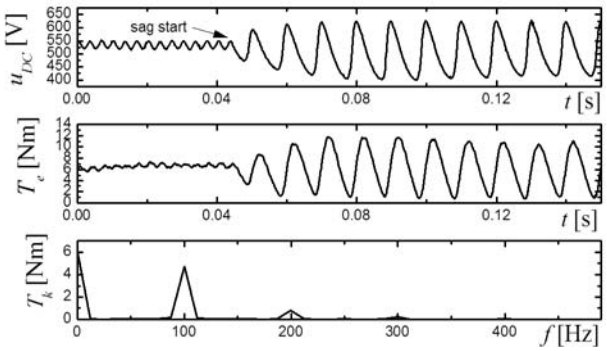

Fig. 9. *B type voltage sag effects on V/Hz drive*

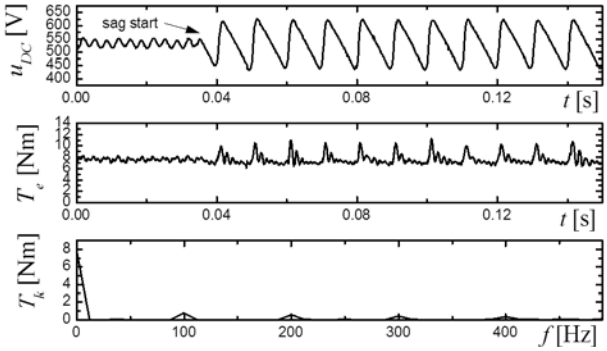

Fig. 10. *B type voltage sag effects on RFO drive*

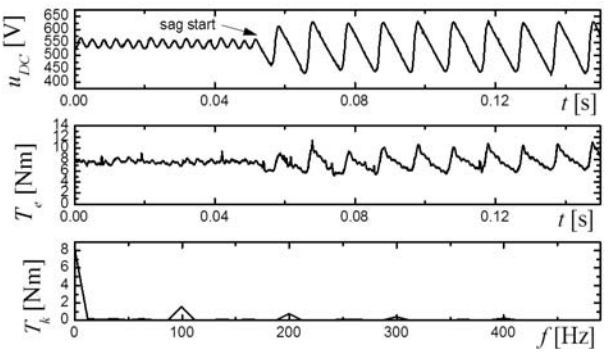

Fig 11. *B type voltage sag effects on PI-DTC drive*

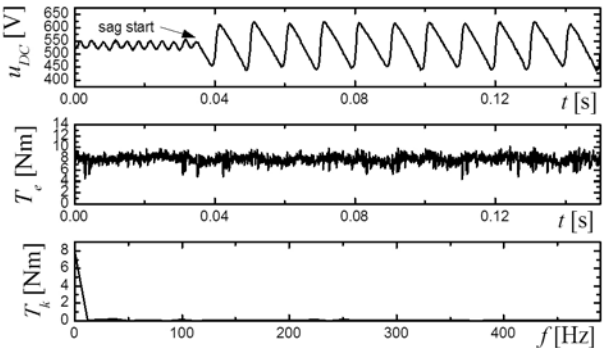

Fig 12. *B type voltage sag effects on C12DTC drive*

reduction was almost three times, which corresponds to the theoretical results from Fig. 8. Twelve sectors DTC drive is submitted to voltage unbalance and in Fig.12 can be seen the expected dc bus voltage ripple, but at the estimated torque practically is not visible the influence. Torque control loop with hysteresis controller efficiently suppresses torque oscillation that is illustrated in the importance in achieving torque recall as fast as possible.

In addition, the torque harmonic spectrum is shown in the Figs. 9-12 as a confirmation of the theoretical analysis carried out. Additional measurements of ASDs vibration can also confirm the previous results (torque harmonic spectrum) and may indicate the possibility of interaction between sag-caused vibrations with purely mechanically induced vibrations at inter-harmonic frequencies.

5. CONCLUSION

Modern adjustable speed drives, regarding to voltage sag, possess different behaviour between the momentary tripping and the partial performance degradation. This paper shows, based on analytical expression and experimental researches, that control algorithm type is with great importance considering unsymmetrical sag effects. Experimental measurements confirmed the theoretically predicted reduction of unwanted harmonic torque. High performance drives (with RFO and DTC algorithm) are less sensible on voltage unbalance, especially drives with traditional DTC technique with hysteresis comparators.

Professional engineers in the field of industrial electric drives can be in the stage of plant system design choose a lower operating speed, which will significantly reduce possible oscillation in torque. Further researches will be conducted on the disturbance observer application in torque/current control loops aimed to additional torque harmonics suppression.

6. REFERENCES

[1] S. Ž. Djokić, K. Stockman, J. V. Milanović, J.J. M. Desmet, and R. Belmans, "Sensitivity of AC adjustable speed drives to voltage sags and short interruptions", *IEEE Trans. Power Delivery*, vol. 20, no. 1, pp. 494–505, Jan. 2005.

[2] M. H. J. Bollen, *Understanding power quality problems: Voltage sags and interruption*s, IEEE Press series on Pwr. Engineering, New York, 2000.

[3] Divan, D.; Luckjiff, G.; Brumsickle, W.; Freeborg, J.; Bhadkamkar, A., "I-grid™: infrastructure for nationwide real-time power monitoring," *Industry Applications Conference, 2002. 37th IAS Annual Meeting. Conference Record of the* , vol.3, no., pp. 1740-1745 vol.3, 2002

[4] K. Lee, T. M. Jahns, W. E. Berkopec and T. A. Lipo, "Closed-form analysis of adjustable speed drive performance under input voltage unbalance and sag conditions", *IEEE Trans. Ind. Appl.,* vol.42, no.3, May/June, 2006, pp. 733-741.

[5] Petronijevic, M.P.; Jeftenic, B.I.; Mitrovic, N.M.; Kostic, V.Z., "Voltage sag drop in speed minimization in modern adjustable speed drives," *Industrial Electronics, 2005. ISIE 2005. Proceedings of the IEEE International Symposium* on , vol.3, no., pp. 929-934 vol. 3, 20-23 June 2005.

[6] D. Telford, M. W. Dunnigan, and B. W. Williams, "Online Identification of Induction Machine Electrical Parameters for Vector Control Loop Tuning," *IEEE Trans. Ind. Electron.*, vol. 50, no. 2, pp. 253-261, April 2003.

[7] Blaabjerg, F.; Kazmierkowski, M.P.; Zelecehowski, M.; Swierczynski, D.; Kolomyjski, W., "Design and comparison direct torque control techniques for induction motors," *Power Electronics and Applications, 2005 European Conference on* , vol., no., pp.9 pp.-P.9, 0-0 0